



# **The Importance of Considering Sub-grid Cloud Variability When Using Satellite Observations to Evaluate the Cloud and Precipitation Simulations in Climate Models**

Hua Song<sup>1</sup>, Zhibo Zhang<sup>1,2\*</sup>, Po-Lun Ma<sup>3</sup>, Steven Ghan<sup>3</sup>, and Minghuai Wang<sup>4</sup>

1. Joint Center for Earth Systems Technology, UMBC, Baltimore, MD
2. Physics Department, UMBC, Baltimore, MD
3. Atmospheric Sciences and Global Change Division, Pacific Northwest National Laboratory, Richland, WA
4. Institute for Climate and Global Change Research & School of Atmospheric Sciences, Nanjing University, Nanjing, China

Corresponding Author:

Dr. Zhibo Zhang

Email: [Zhibo.Zhang@umbc.edu](mailto:Zhibo.Zhang@umbc.edu)

Phone: +1 (410) 455 6315



## Abstract

Satellite cloud observations have become an indispensable tool for evaluating the general circulation models (GCMs). To facilitate the satellite and GCM comparisons, the CFMIP (Cloud Feedback Model Inter-comparison Project) Observation Simulator Package (COSP) has been developed and is now increasingly used in GCM evaluations. In this study, we use COSP cloud simulations from the Super-Parameterized Community Atmosphere Model (SPCAM5) and satellite observations from the Moderate Resolution Imaging Spectroradiometer (MODIS) and CloudSat to demonstrate the importance of considering the sub-grid variability of cloud and precipitation when using the COSP to evaluate GCM simulations. We carry out two sensitivity tests: SPCAM5 COSP and SPCAM5-Homogeneous COSP. In the SPCAM5 COSP run, the sub-grid cloud and precipitation properties from the embedded cloud resolving model (CRM) of SPCAM5 are used to drive the COSP simulation, while in the SPCAM5-Homogeneous COSP run only grid mean cloud and precipitation properties (i.e., no sub-grid variations) are given to the COSP. We find that the warm rain signatures in the SPCAM5 COSP run agree with the MODIS and CloudSat observations quite well. In contrast, the SPCAM5-Homogeneous COSP run which ignores the sub-grid cloud variations, substantially overestimates the radar reflectivity and probability of precipitation compared to the satellite observations, as well as the results from the SPCAM5 COSP run. The significant differences between the two COSP runs demonstrate that it is important to take into account the sub-grid variations of cloud and precipitation when using COSP to evaluate the GCM to avoid confusing and misleading results.



## 49 1. Introduction

50 Marine boundary layer (MBL) cloud, as a strong modulator of the radiative energy  
51 budget of the Earth-Atmosphere system, is a major source of uncertainty in future climate  
52 change projections of the general circulation models (GCM) (Cess et al., 1996; Bony and  
53 Dufresne, 2005). Improving MBL cloud simulations in the GCMs is one of the top priorities of  
54 the climate modeling community. As the cloud parameterization schemes in the GCMs become  
55 increasingly sophisticated, there is a strong need for comprehensive global satellite cloud  
56 observations for model evaluation and improvement. However, the fundamental definitions of  
57 clouds in GCMs differ dramatically from those used for satellite remote sensing, which hampers  
58 the use of satellite products for model evaluation. In order to overcome this obstacle, the Cloud  
59 Feedback Model Inter-comparison Project (CFMIP) community has developed an integrated  
60 satellite simulator, the CFMIP Observation Simulator Package (COSP) (Zhang et al., 2010;  
61 Bodas-Salcedo et al., 2011). COSP has greatly facilitated and promoted the use of satellite data  
62 in the climate modeling community to expose and diagnose issues in GCM cloud simulations  
63 (e.g., Marchand et al., 2009; Zhang et al., 2010; Kay et al., 2012; Pincus et al., 2012; Kay et al.,  
64 2016; Song et al., 2017).

65 Warm rain is a unique and important feature of MBL clouds. It plays an important role in  
66 determining the macro- and micro-physical properties of MBL clouds, in particular, the cloud  
67 water budget (e.g., Stevens et al., 2005; Wood, 2005; Comstock et al., 2005). Many previous  
68 studies have investigated the warm rain simulation in GCMs using the COSP simulators. These  
69 studies reveal a common problem in the latest generation of GCMs, i.e., the drizzle in MBL  
70 clouds is too frequent in the GCM compared with satellite observations (e.g., Zhang et al. 2010;  
71 Franklin et al. 2013; Suzuki et al. 2015; Takahashi et al., 2017; Jing et al., 2017; Song et al.,



2017, Bodas-Salcedo et al. 2008; Stephens et al. 2010; Bodas-Salcedo et al. 2011; Nam and  
Quaas 2012; Franklin et al. 2013; Jing et al., 2017). One possible reason for the excessive warm  
rain production in GCMs could be the model's inaccurate representation of physical processes,  
such as auto-conversion and accretion that govern the precipitation efficiency in warm MBL  
clouds. Due to the lack of sub-grid variability of microphysical quantities in most large-scale  
models, the auto-conversion parameterization is overly aggressive so that the models tend to  
produce precipitation too quickly (Lebsock et al. 2012, 2013, Song et al. 2017).

The radar observations of warm rain from CloudSat and collocated MODIS (Moderate  
Resolution Imaging Spectroradiometer) cloud observations are extremely useful data for  
assessing and improving the GCM simulations of MBL clouds and their precipitation process.  
However, the dramatic spatial resolution differences between the conventional GCM (~100km)  
and satellite observations (~1km) become a challenging obstacle for the satellite and GCM  
comparisons. To overcome this obstacle, the COSP first divides the grid-level cloud and  
precipitation properties (e.g., grid-mean cloud water and rain water) into the so-called “sub-  
columns” that are conceptually similar to “pixel” in satellite observation. Then for each sub-  
column the COSP satellite-simulators (e.g., COSP-CloudSat and COSP-MODIS) simulate the  
satellite measurements (e.g., radar reflectivity) and retrievals (e.g., MODIS cloud optical depth  
and effective radius) which become directly comparable with satellite data. Ideally, the sub-  
column generation in COSP should be consistent with the sub-grid cloud parameterization  
scheme in the host GCM. However, in practice sub-grid variations of cloud and precipitation are  
often ignored or treated crudely in the COSP simulation for a number of possible reasons. First  
of all, the COSP is an independent package and it takes substantial efforts to implement in the  
COSP a sub-grid cloud generation scheme that is consistent with the host GCM. Secondly, a





95 simple sub-column generation scheme helps alleviate the computational cost associated with the  
96 COSP simulation. Last but certainly not least, the users of the COSP might not be fully aware of  
97 the consequences of ignoring the sub-grid cloud and precipitation variability in the COSP  
98 simulations.

99 The current version (v1.4) of COSP provides a built-in highly simplified sub-column  
100 generator. It accounts only for the sub-grid variability of the types of hydrometeors and ignores  
101 the variability of mass and microphysics within each hydrometeor type. The water content and  
102 microphysical properties (i.e., droplet effective radius and optical thickness) of each hydrometeor  
103 are horizontally homogenous among all the sub-columns that are labeled as the same type (i.e.,  
104 stratiform or convective). Here we refer to the current scheme as the “*homogenous hydrometeor*  
105 *scheme*”. The uncertainties and potential biases caused by the *homogenous hydrometeor scheme*  
106 can be significant and should not be overlooked. A simple hypothetical example is provided in  
107 Figure 1 to illustrate the importance of accounting for the sub-grid variability of rainwater in  
108 simulating the CloudSat radar reflectivity. To be consistent with the two-moment cloud  
109 microphysics scheme (Morrison and Gettelman, 2008) that is widely used in the GCMs, we  
110 assume the sub-grid distribution of rainwater to follow the exponential distribution. In this  
111 example, the grid-mean rainwater mixing ratio ( $\bar{q}$ ) is set to be 0.03 g/kg (dashed blue line in  
112 Figure 1a). Using the Quickbeam simulator (Haynes et al., 2007) in COSP, we simulated the  
113 corresponding 94-GHz CloudSat radar reflectivity, which is shown in Figure 1b. The grid-mean  
114 radar reflectivity based on the exponentially distributed rainwater (i.e., with sub-grid variance) is  
115 about 4 dBZ (solid red line in Figure 1b). In contrast, if the sub-grid variation of rainwater is  
116 ignored, the radar reflectivity corresponding to  $\bar{q} = 0.03$  g/kg is 13 dBZ (dashed blue line in  
117 Figure 1b). The substantial difference between the two indicates that ignoring the sub-grid



118 variability of hydrometeors could cause significant overestimation of grid-mean radar reflectivity  
119 simulation, which in turn could complicate and even mislead the evaluation of GCMs.

120 The objective of this study is to investigate and demonstrate to the GCM modeling  
121 community the importance of considering the sub-grid variability of cloud and precipitation  
122 properties when evaluating the GCM simulations using COSP. Here we employ the Super-  
123 parameterized Community Atmosphere Model Version 5 (SPCAM5, Wang et al., 2015) to  
124 provide the sub-grid cloud and precipitation hydrometeor fields for a comparison study of the  
125 simulated radar reflectivity and warm rain frequencies by COSP. Fundamentally different from  
126 the convective cloud parameterization schemes in GCMs, SPCAM5 consists of a two-  
127 dimensional cloud-resolving model (CRM) embedded into each grid of a conventional CAM5  
128 (Khairoutdinov and Randall, 2003; Wang et al., 2015). The sub-grid cloud dynamical and  
129 microphysical processes are explicitly resolved at a 4-km resolution in SPCAM5. We carry out  
130 two sensitivity tests: SPCAM5 COSP and SPCAM5-Homogeneous COSP. In the SPCAM5  
131 COSP run, the sub-grid cloud and precipitation properties from the embedded CRMs of  
132 SPCAM5 are used to drive the COSP simulation. In the SPCAM5-Homogeneous COSP run, the  
133 default *homogenous hydrometeor scheme* of COSP mentioned above is used to generate the sub-  
134 grid cloud and precipitation fields for the COSP simulation. The outputs from the two runs are  
135 compared with the collocated CloudSat and MODIS observations to assess the potential  
136 problems in both runs, and also to understand the impacts of omitting sub-grid cloud variations  
137 in the COSP simulations.

138 The rest of the paper is organized as follows: Section 2 describes the model, COSP and  
139 satellite data used in this study. Results are represented in Section 3. Finally, Section 4 provides  
140 general conclusions and remarks.



141

## 142 **2. Description of Model, COSP and Satellite Observations**

### 143 **2.1. Model**

144 The model used in this study is SPCAM5, an application of the Multiscale Modeling  
145 Framework (MMF) (Randall et al., 2003; Khairoutdinov et al., 2005, 2008; Tao et al., 2009) to  
146 CAM5 (Neale et al., 2010), which uses the finite volume dynamical core at  $1.9^\circ$  latitude  $\times$   $2.5^\circ$   
147 longitude resolution with 30 vertical levels and 600-s time step. The embedded 2-D CRM in  
148 each CAM5 grid cell includes 32 columns at 4 km horizontal grid spacing and 28 vertical layers  
149 coinciding with the lowest 28 CAM5 levels. The CRM runs with a 20-s time step. Details of the  
150 SPCAM5 can be found in Wang et al. (2011; 2015). The simulations are run in a “constrained  
151 meteorology” configuration (Ma et al., 2013; 2015) to facilitate model evaluation against  
152 observations, in which the model winds are nudged toward the Modern Era Reanalysis for  
153 Research Applications (MERRA) reanalysis with a relaxation timescale of 6 hours (Zhang et al.,  
154 2014). The SPCAM5 simulations are performed from September 2008 to December 2010 (28  
155 months). The last 24 months (January 2009–December 2010) outputs of the simulations are used  
156 for analysis.

### 157 **2.2. COSP**

158 We used COSP Version 1.4, which has no scientific difference from the latest version  
159 COSP2 (Swales et al., 2018). Currently, COSP provides simulations of ISCCP (International  
160 Satellite Cloud Climatology Project), CALIPSO (Cloud-Aerosol Lidar and Infrared Pathfinder  
161 Satellite Observation), CloudSat, MODIS, and MISR (Multi-angle Imaging SpectroRadiometer)  
162 cloud measurements and/or retrievals (Bodas-Salcedo et al., 2011). In this study, we will focus  
163 on the MODIS and CloudSat simulators (Pincus et al., 2012; Haynes et al., 2007). COSP has



164 three major parts, each controlling a step of the pseudo-retrieval process: (1) the *sub-column*  
165 *generator* of COSP first distributes the grid-mean cloud and precipitation properties from GCM  
166 into the so-called sub-columns that are conceptually similar to “pixels” in satellite remote  
167 sensing. (2) the *satellite simulators* simulate the direct measurements (e.g., CloudSat radar  
168 reflectivity and CALIOP backscatter) and retrieval products (e.g., MODIS cloud optical  
169 thickness and effective radius) for each sub-column using highly simplified radiative transfer and  
170 retrieval schemes; (3) the *aggregation scheme* averages the sub-column simulations back to grid  
171 level to obtain temporal-spatial averages that are comparable with aggregated satellite products  
172 (e.g., MODIS level-3 gridded monthly mean products).

173 As mentioned in the Introduction, the COSP-v1.4 has a highly simplified built-in sub-  
174 column generator based on the homogenous hydrometeor scheme. This scheme accounts only for  
175 the sub-grid variability of the types of hydrometeors and ignores the variability of mass and  
176 microphysics within each hydrometeor type. An example is provided in Figure 2 to illustrate  
177 how this default sub-column generator of COSP-v1.4 distributes the grid-mean cloud and  
178 precipitation into the sub-columns. We arbitrarily selected a grid (23°N and 150°E) with both  
179 cloud and significant precipitation from our previous CAM5 simulations (Song et al., 2017).  
180 Figure 2a shows the vertical profiles of the grid-mean total (stratiform plus convective) and  
181 convective cloud fractions at the selected grid box. Figure 2b shows the vertical profiles of the  
182 grid-mean mixing ratios of each type of hydrometeors. The sub-column generator of COSP takes  
183 the grid-mean cloud fractions, hydrometeor mixing ratios and effective particle sizes (Figure 2a  
184 and Figure 2b) as inputs to generate the sub-columns for the later satellite measurement and  
185 retrieval simulation.



186 First, sub-columns (150 sub-columns generated in our example) are assigned as either  
187 cloudy or clear at each model level by the Subgrid Cloud Overlap Profile Sampler (SCOPS),  
188 which was developed originally as part of the ISCCP simulator (Klein and Jakob, 1999; Webb et  
189 al., 2001). As illustrated in Figure 2c, the SCOPS assigns cloud to the sub-columns in a manner  
190 consistent with the model's grid box average stratiform and convective cloud amounts (Figure  
191 2a) and its cloud overlap assumption, i.e., maximum-random overlap in this case. The next step  
192 is to determine which of the sub-columns generated by SCOPS contain precipitation  
193 hydrometeors, e.g., rain and snow. This step is necessary and critical for the COSP CloudSat  
194 radar simulator (Bodas-Salcedo et al., 2011) because radar reflectivity is highly sensitive to the  
195 precipitation hydrometeors due to their large particle size (L'Ecuyer and Stephens, 2002; Tanelli  
196 et al., 2008). The current sub-grid precipitation distribution scheme "SCOPS-PREC" is  
197 developed and described in Zhang et al. (2010). Figure 2d shows the masking of precipitation  
198 among the 150 sub-columns generated by the SCOPS-PREC for the example grid. After the  
199 cloud and precipitation are masked, the last step is to specify the mass (i.e., mixing ratio) and  
200 effective radius of hydrometeors for all the sub-columns occupied by clouds and/or precipitation.  
201 The current scheme for this step is highly simplified. As shown in Figure 2e, it assumes the mass  
202 and the microphysics of each type of hydrometeor to be horizontally homogeneous among all the  
203 sub-columns that are occupied by this type of hydrometeor at a given model level. In other  
204 words, at each model level the only difference among sub-columns is that they may be occupied  
205 by different types of hydrometeors (Zhang et al., 2010).

206 In this study, we have carried out two COSP simulations using the 2-year SPCAM5  
207 CRM outputs to investigate the importance of considering the sub-grid variations of cloud and  
208 precipitation properties when evaluating the GCM simulations using COSP. The two COSP



simulations are marked as SPCAM5 COSP and SPCAM5-Homogeneous COSP, respectively. For the SPCAM5 COSP simulation, we treat the sub-grid cloud and precipitation fields from the CRM of SPCAM5 outputs as sub-columns of COSP without using the COSP sub-column generator. For the SPCAM5-Homogeneous COSP simulation, we first average the sub-grid cloud and precipitation fields (including both clear and cloudy sub-grids) from the CRM of SPCAM5 to each CAM5 grid, and then input these grid-mean cloud and precipitation fields to the default COSP-v1.4 sub-column simulator described above to generate the sub-column fields. All the other processes of two COSP simulations are exactly same. The COSP simulator outputs are produced from 6-hourly calculations and the number of sub-columns used here is 32. To derive the probability of precipitation, we made some simple in-house modifications in COSP v1.4 to write out the MODIS and CloudSat simulations for every sub-column. This allows us to derive the joint statistics of COSP-MODIS and COSP-CloudSat simulations and compare them with those derived from collocated MODIS and CloudSat level-2 products.

### 2.3. Satellite Data

The cloud measurements from the A-Train satellite sensors, namely MODIS and CloudSat, are used for model-to-observation comparison. The newly released collection 6 (C6) Aqua-MODIS cloud products (Platnick et al., 2017) are used to evaluate cloud fraction, cloud optical thickness and cloud droplet effective radius. For MBL cloud studies, CloudSat provides valuable information on the warm rain process that cannot be achieved by a passive sensor like MODIS. The direct measurement of CloudSat is the vertical profile of 94-GHz radar reflectivity by cloud and hydrometer particles (i.e., 2B-GEOPROF product), from which other information such as vertical distribution of clouds and precipitation can be derived. The CloudSat 2B-GEOPROF product (Marchand et al., 2008) is used for cloud vertical structure, radar reflectivity,



232 and identification of precipitation in MBL clouds. To prepare for the comparison of joint  
233 statistics, we collocated 5 years (2006 ~ 2010) of pixel-level (i.e., level-2) MODIS and CloudSat  
234 observations using the collocation scheme developed in Cho et al. (2008). Due to the low  
235 sampling rate of CloudSat, we used 5 years (2006 ~ 2010) of observations, in comparison with  
236 the 2-year model simulation (2009 ~ 2010), to obtain enough statistics. A sensitivity study  
237 indicates that the inter-annual variability of MBL clouds is much smaller than the model-to-  
238 observation differences.

239 In this study, we focus on the tropical and subtropical regions between 45°S and 45°N  
240 (loosely referred to as “tropical and subtropical region”), where most stratocumulus and cumulus  
241 regimes are found. We avoid high latitudes because satellite observations, namely MODIS, may  
242 have large uncertainties to low solar zenith angles there (Kato and Marshak, 2009; Grosvenor  
243 and Wood, 2014; Cho et al., 2015).

244

### 245 **3. Sensitivity Study: SPCAM5 COSP vs. SPCAM5-Homogeneous COSP**

246 First, we compare the Contoured Frequency by Altitude Diagram (CFAD) of tropical  
247 clouds derived based on SPCAM5 COSP and SPCAM5-Homogeneous COSP simulations with  
248 that derived from CloudSat 2B-GEOPROF product in Figure 3. The CFAD based CloudSat  
249 observations displays a typical boomerang type shape that has been reported in many previous  
250 studies (Bodas-Salcedo et al., 2011; Zhang et al., 2010; Marchand et al., 2009). Focusing on the  
251 low clouds below 3km, we observe a rather broad distribution of radar reflectivity with a  
252 maximum occurrence frequency around -30 dBZ ~ -20 dBZ followed by a long tail extending to  
253 about 10 dBZ. As pointed out in previous studies, the peak around -30 dBZ ~ -20 dBZ is due to  
254 non-precipitating MBL clouds and the precipitating clouds with increasing rain rate give rise to



the long tail. The CFAD based on two COSP simulations exhibits some characteristics similar to the CloudSat observations, but also many noticeable differences. In particular, the two COSP simulations both produce a much narrower range of radar reflectivity for low clouds, with occurrence frequency clustered mostly around  $-25$  dBZ in SPCAM5 COSP and around  $0$  dBZ in SPCAM5-Homogeneous COSP. These results show that using the oversimplified COSP sub-column generator (e.g., the homogeneous hydrometeor scheme) has non-negligible influences on the simulated radar reflectivity and produces artificially high occurrences of large radar reflectivity.

The systematic biases in simulated radar reflectivity by the COSP homogeneous hydrometeor scheme might lead to the unjustified and biased evaluation of the warm rain production in GCMs, since cloud column maximum radar reflectivity ( $Z_{\max}$ ) is often used to distinguish precipitating from non-precipitating MBL clouds (Kubar and Hartmann, 2009; Lebsock and Su, 2014; Haynes et al., 2009).

Next we compare the simulated and observed PDFs of  $Z_{\max}$  for all the sub-columns that are marked as warm liquid clouds in the domain between  $45^{\circ}\text{S}$  and  $45^{\circ}\text{N}$ . The warm liquid clouds are defined by the cloud phase and cloud top pressure derived from the MODIS simulator by the criteria that cloud phase is liquid and cloud top pressure is between  $900$  hPa and  $500$  hPa. Big differences in the PDFs of  $Z_{\max}$  between the SPCAM5-Homogeneous COSP and the A-Train observations, and between SPCAM5-Homogeneous COSP and SPCAM5 COSP are shown in Figure 4. First, in the A-Train observations, about 46% of warm liquid clouds detected by the MODIS are not observed by the CloudSat. These clouds are either too thin and therefore their radar reflectivity is too weak to be detected by CloudSat, or they are too low and therefore suffer the surface clutter issue (Marchand et al., 2008). For those warm liquid clouds detected by both





the MODIS and CloudSat, the PDF of  $Z_{\max}$  peaks around -25 dBZ. Second, in both COSP simulations, almost all warm liquid clouds derived by the MODIS simulator have valid CloudSat radar reflectivity larger than -40 dBZ. The PDFs of  $Z_{\max}$  in the SPCAM5 reasonably resemble those in the A-Train observations. However, significantly different from the other two, the distribution of  $Z_{\max}$  in the SPCAM5-Homogeneous shifts to the large dBZ values and peaks around 0 dBZ. In previous studies (e.g., Takahashi et al., 2017), warm liquid clouds are categorized to three different modes by  $Z_{\max}$ : non-precipitating mode ( $Z_{\max} < -15$  dBZ), drizzle mode ( $-15$  dBZ  $< Z_{\max} < 0$  dBZ) and rain mode ( $Z_{\max} > 0$  dBZ). The simulated and observed PDFs of  $Z_{\max}$  demonstrate that a large portion of warm liquid clouds is non-precipitating in the observations and SPCAM5 COSP while most warm liquid clouds are precipitating (drizzle or rain) clouds in the SPCAM5-Homogeneous COSP. The use of the COSP homogeneous hydrometeor scheme gives us a dramatically different assessment of the warm rain production of MBL clouds in the SPCAM5 model, i.e., if we consider the sub-column variability of cloud and precipitation in the COSP simulation, we find that the SPCAM5 model can reproduce the observed warm rain production quite well. However, if we ignore the CRM sub-grid variability and use the homogeneous hydrometeor scheme, we may make the biased conclusion that the SPCAM5 model performs badly in the simulation of warm rain production.

More significant differences between the SPCAM5 COSP and SPCAM5-Homogeneous COSP simulations can be found from the spatial distributions of the probability of precipitation (POP) in MBL warm clouds (Figure 5). Here, the POP for a given grid box is defined as the fraction of liquid-phase cloud identified by MODIS observations with  $Z_{\max}$  larger than a certain threshold (i.e., -15 dBZ for drizzle or rain, 0 dBZ for rain, and 10 dBZ for heavy rain, respectively) according to the collocated CloudSat observations with respect to the total



301 population liquid-phase clouds with the cloud top pressure between 500 hPa and 900 hPa in the  
302 grid. Observations in Figure 5 suggest that roughly a third of MBL clouds observed by MODIS  
303 in the tropical and subtropical region are likely precipitating (drizzle or rain), with a domain  
304 averaged POP around 33%. The POP of drizzle plus rain has a distinct pattern: smaller (~15%)  
305 in the coastal Sc regions and increasing to ~50% in the Cu cloud regions. The observed POPs of  
306 rain and heavy rain show similar spatial patterns as those of drizzle plus rain, with much smaller  
307 domain averaged POP being about 12.5% and 3.3%, respectively.

308 In the same way as we define POP for observations, we define the POP for two COSP  
309 simulations as the ratio of sub-columns that have COSP-CloudSat simulated  $Z_{\max}$  larger than a  
310 certain threshold with respect to the total number of liquid-phase clouds identified by COSP-  
311 MODIS. As shown in Figure 5, two COSP simulations show dramatically different spatial  
312 distributions of POPs. The SPCAM5 COSP produces the similar POP patterns as those in the  
313 observations, with the domain averaged POPs for drizzle or rain, rain and heavy rain being about  
314 43%, 16% and 4.5%, respectively. However, the POPs in the SPCAM5-Homogeneous COSP are  
315 substantially overestimated, with the domain averaged POPs for drizzle or rain, rain and heavy  
316 rain being about 75%, 36% and 7%, respectively. Using the COSP homogeneous hydrometeor  
317 scheme will lead to the conclusion that the drizzle or rain is triggered too frequently (more than  
318 double of the observations) in the SPCAM5 model, which obviously is not a fair assessment.

319 Previous studies find that the warm rain production in MBL clouds is tightly related to  
320 the in-cloud microphysical properties of MBL clouds (e.g., Stevens et al., 2005; Wood, 2005;  
321 Comstock et al., 2005). Next, we check the dependence of POP on in-cloud properties liquid  
322 water path (LWP) and on liquid cloud effective radius ( $r_e$ ) in both observations and two COSP  
323 simulations. Figure 6 shows the POPs of drizzle or rain (i.e.,  $Z_{\max} > -15$  dBZ) as a function of in-



cloud LWP and  $r_e$  overlaid by the joint PDF of LWP and  $r_e$  (white contours) in the satellite observations and two COSP simulations. The observed POPs of warm liquid clouds increase monotonically with increasing in-cloud LWP and  $r_e$ , with high POPs concentrating on the domain with large values of LWP and  $r_e$  (i.e.,  $LWP > 200 \text{ g/m}^2$  and  $r_e > 15 \text{ }\mu\text{m}$ ). However, in the two COSP simulations, especially the SPCAM5-Homogeneous COSP, at each joint bin the POPs are much larger than those in the A-Train observations. When in-cloud LWP ( $r_e$ ) is larger than  $150 \text{ g/m}^2$  ( $17 \text{ }\mu\text{m}$ ), the dependence of POPs on in-cloud  $r_e$  (LWP) is small. The joint PDFs of in-cloud LWP and  $r_e$  in the observations and two COSP simulations are also quite different. There are more occurrences with large LWP and  $r_e$  in the MODIS observations than the two COSP simulations. The SPCAM5 COSP simulations have two peaks of the joint PDFs, which are converted to one occurrence peak in the SPCAM5-Homogeneous COSP simulation by using the COSP homogeneous hydrometeor scheme.

Based on the above comparisons, we can see that the oversimplified COSP sub-column generator contributes to not only the narrow distribution of MBL cloud radar reflectivity, but also to unrealistically high POPs in the SPCAM5 model. Besides, it also changes the distribution of in-cloud microphysical properties, and the relationship between POPs and cloud microphysical properties as well.

341

#### 342 **4. Summary and Discussion**

This study presents a satellite-based evaluation of the warm rain production of MBL cloud in the SPCAM5 model using two COSP simulations (SPCAM5 COSP and SPCAM5-Homogeneous COSP), with the objective to demonstrate the importance of considering the sub-grid variability of cloud and precipitation when using COSP to evaluate GCM simulations.



347 Through the SPCAM5 COSP simulations, in which the sub-column variability of cloud and  
348 precipitation is considered, we find that the SPCAM5 model can reproduce the observed warm  
349 rain production quite well. However, in the SPCAM5-Homogeneous COSP simulation, in which  
350 we ignore the CRM sub-grid variability and use the COSP homogeneous hydrometeor scheme,  
351 the simulated radar reflectivity and POPs in the SPCAM5 are significantly overestimated  
352 compared to the observations. Therefore, use of the COSP homogeneous hydrometeor scheme  
353 gives us a significantly different assessment of warm rain production of MBL clouds in the  
354 SPCAM5 model.

355 The systematic and significant biases due to the limitation of current homogeneous  
356 hydrometeor scheme can mislead the evaluation of GCMs and should not be overlooked. In this  
357 regard, an improved sub-column generator needs to be developed for COSP to account for the  
358 sub-grid variances of cloud and/or hydrometer mass and microphysics. A recent study of  
359 Hillman et al. (2017) investigated the sensitivities of simulated satellite retrievals to subgrid-  
360 scale overlap and condensate heterogeneity, and demonstrated the systematic biases in the  
361 simulated MODIS cloud fraction and CloudSat radar reflectivity due to the oversimplified COSP  
362 sub-column generator. Their study also proposed a new scheme to replace the COSP current  
363 sub-column generator, and showed that the new scheme can produce much better satellite  
364 retrievals. Implementing their sub-column heterogeneous hydrometeor scheme in COSP may  
365 improve the GCM COSP simulations and give a better-justified assessment of the GCM  
366 performance in simulating warm rain processes and cloud microphysical properties.

367 On the other hand, since the assumptions of sub-grid variability of cloud and  
368 hydrometeors in different GCMs may be quite different, one universal sub-column hydrometeor  
369 scheme may be not applicable to all models. Based on this consideration, the latest version



370 COSP version 2 enhances flexibility by allowing for model-specific representation of sub-grid  
371 scale cloudiness and hydrometeor condensates and encourages the users to implement the same  
372 sub-grid scheme as the host GCM for consistency (Swales et al., 2018). Nevertheless, our study  
373 also suggests that any evaluation study of warm rain production in GCMs by using COSP  
374 simulators should take this issue into account.

375

376

377

#### 378 **Code and Data Availability:**

379 Details of SPCAM5 can be found in Wang et al. (2011). The host GCM in SPCAM5 is  
380 the Community Atmospheric Model, Version 5 (see details on the CESM website at  
381 <http://www.cesm.ucar.edu/models/cesm1.1/cam/>). SPCAM5 has recently been merged with  
382 CESM1.1.1 and released to the public (Randall et al., 2013; [https://svn-ccsm-](https://svn-ccsm-release.cgd.ucar.edu/model_development_releases/spcam2_0-cesm1_1_1)  
383 [release.cgd.ucar.edu/model\\_development\\_releases/spcam2\\_0-cesm1\\_1\\_1](https://svn-ccsm-release.cgd.ucar.edu/model_development_releases/spcam2_0-cesm1_1_1)). Codes of COSP V1.4  
384 can be found in the website at <https://github.com/CFMIP/COSPv1>. We used the collection 6 (C6)  
385 Aqua-MODIS cloud products (Platnick et al., 2017), which can be downloaded from the NASA  
386 website at [https://ladsweb.modaps.eosdis.nasa.gov/api/v1/productPage/product=MYD06\\_L2](https://ladsweb.modaps.eosdis.nasa.gov/api/v1/productPage/product=MYD06_L2).  
387 The CloudSat data are distributed by the CloudSat Data Processing Center. The CloudSat 2B-  
388 GEOPROF product we used is downloaded from the website at  
389 <http://www.cloudsat.cira.colostate.edu/data-products/level-2b/2b-geoprof?term=42>.

390

391

392



393 **Acknowledgements.** This research is supported by Department of Energy (DOE), Office of  
394 Science, Biological and Environmental Research, Regional & Global Climate Modeling Program  
395 (grant #DE-SC0014641). The Pacific Northwest National Laboratory is operated for the DOE by  
396 Battelle Memorial Institute under contract DE-AC05-76RLO 1830. Minghuai Wang was  
397 supported by the Minister of Science and Technology of China (2017YFA0604001). The  
398 computations in this study were performed at the UMBC High Performance Computing Facility  
399 (HPCF). The facility is supported by the U.S. National Science Foundation through the MRI  
400 program (grant nos. CNS-0821258 and CNS-1228778) and the SCREMS program (grant no.  
401 DMS-0821311), with substantial support from UMBC. The MODIS cloud products used in this  
402 study are downloaded from NASA Level-1 and Atmosphere Archive and Distribution System  
403 (<https://ladsweb.modaps.eosdis.nasa.gov/>). The CloudSat products are provided by CloudSat  
404 Data Processing Center (<http://www.cloudsat.cira.colostate.edu/>).

405

406

407

408

409

410

411

412

413

414

415



## 416 Reference

- 417 Bodas-Salcedo, A., and Coauthors, 2011: COSP: Satellite simulation software for model  
418 assessment. *Bull. Am. Meteorol. Soc.*, **92**, 1023–1043, doi:10.1175/2011BAMS2856.1.
- 419 Bony, S., and J.-L. Dufresne, 2005: Marine boundary layer clouds at the heart of tropical cloud  
420 feedback uncertainties in climate models. *Geophys. Res. Lett.*, **32**, L20806,  
421 doi:10.1029/2005GL023851.
- 422 Cess, R., and Coauthors, 1996: Cloud feedback in atmospheric general circulation models: An  
423 update. *J. Geophys. Res. Atmos.*, **101**, 12791–12794.
- 424 Cho, H. M., P. Yang, G. W. Kattawar, S. L. Nasiri, Y. Hu, P. Minnis, C. Trepte, and D. Winker,  
425 2008: Depolarization ratio and attenuated backscatter for nine cloud types: Analyses based  
426 on collocated CALIPSO lidar and MODIS measurements, *Opt. Express*, **16**(6), 3931–3948.
- 427 Cho, H. M., and Coauthors, 2015: Frequency and causes of failed MODIS cloud property  
428 retrievals for liquid phase clouds over global oceans. *J. Geophys. Res. Atmos.*, **120**,  
429 2015JD023161–n/a, doi:10.1002/2015JD023161.
- 430 Comstock, K. K., C. S. Bretherton, and S. E. Yuter, 2005: Mesoscale variability and drizzle in  
431 southeast Pacific stratocumulus. *J. Atmos. Sci.*, **62**, 3792–3807, doi:10.1175/JAS3567.1.
- 432 Franklin, C. N., Z. Sun, D. Bi, M. Dix, H. Yan, and A. Bodas-Salcedo, 2013: Evaluation of  
433 clouds in access using the satellite simulator package COSP: regime-sorted tropical cloud  
434 properties. *J. Geophys. Res. Atmos.*, **118**(12), 6663–6679, doi: 10.1002/jgrd.50496.
- 435 Grosvenor, D. P., and R. Wood, 2014: The effect of solar zenith angle on MODIS cloud optical  
436 and microphysical retrievals within marine liquid water clouds. *Atmospheric Chemistry and  
437 Physics*, **14**, 7291–7321, doi:10.5194/acpd-14-303-2014.
- 438 Haynes, J. M., T. S. L'Ecuyer, G. L. Stephens, S. D. Miller, C. Mitrescu, N. B. Wood, and S.  
439 Tanelli, 2009: Rainfall retrieval over the ocean with spaceborne W-band radar. *J. Geophys.  
440 Res. Atmos.*, **114**, doi:10.1029/2008JD009973.
- 441 Hillman, B. R., R. T. Marchand, and T. P. Ackerman, 2017: Sensitivities of simulated satellite  
442 views of clouds to subgrid-scale overlap and condensate heterogeneity, *J. Geophys. Res.  
443 Atmos.*, under revision.
- 444 Jakob, C., and S. A. Klein, 2000: A parameterization of the effects of cloud and precipitation  
445 overlap for use in general-circulation models, *Quarterly Journal of the Royal  
446 Meteorological Society*, **126**(568), 2525–2544, doi:10.1002/qj.49712656809.
- 447 Jing, X., K. Suzuki, H. Guo, D. Goto, T. Ogura, T. Koshiro, and J. Mülmenstädt, 2017: A  
448 multimodel study on warm precipitation biases in global models compared to satellite  
449 observations. *J. Geophys. Res. Atmos.*, **122**, <https://doi.org/10.1002/2017JD027310>.



- 450 Kato, S., and A. Marshak, 2009: Solar zenith and viewing geometry dependent errors in satellite  
451 retrieved cloud optical thickness: Marine Scase. *J. Geophys. Res. Atmos.*, **114**, D01202,  
452 doi:10.1029/2008JD010579.
- 453 Kay, J. E., and Coauthors, 2012: Exposing global cloud biases in the community atmosphere  
454 model (CAM) using satellite observations and their corresponding instrument simulators. *J.*  
455 *Climate*, **25**, 5190–5207, doi:10.1175/JCLI-D-11-00469.1.
- 456 Kay, J. E., Tristan L’Ecuyer, Helene Chepfer, Norman Loeb, Ariel Morrison, and Gregory  
457 Cesana, 2016: Recent Advances in Arctic Cloud and Climate Research. *Current Climate*  
458 *Change Reports*, **2**, 159–169.
- 459 Khairoutdinov, M., and Y. Kogan, 2000: A new cloud physics parameterization in a large-eddy  
460 simulation model of marine stratocumulus, *Mon. Wea. Rev.*, **128**, 229–243.
- 461 Khairoutdinov, M. F., and D. A. Randall, 2003: Cloud resolving modeling of the ARM summer  
462 1997 IOP: Model formulation, results, uncertainties, and sensitivities, *J. Atmos. Sci.*, **60**(4),  
463 607–625.
- 464 Khairoutdinov, M., D. Randall, and C. DeMott, 2005: Simulations of the atmospheric general  
465 circulation using a cloud-resolving model as a superparameterization of physical processes, *J.*  
466 *Atmos. Sci.*, **62**(7), 2136–2154.
- 467 Khairoutdinov, M., C. DeMott, and D. Randall, 2008: Evaluation of the simulated interannual  
468 and subseasonal variability in an AMIP-style simulation using the CSU multiscale modeling  
469 framework, *J. Climate*, **21**(3), 413–431.
- 470 Klein, S. A., Y. Zhang, M. D. Zelinka, R. Pincus, J. Boyle, and P. J. Gleckler, 2013: Are climate  
471 model simulations of clouds improving? An evaluation using the ISCCP simulator. *J.*  
472 *Geophys. Res. Atmos.*, **118**, 1329–1342, doi:10.1002/jgrd.50141.
- 473 Klein, S., and D. Hartmann, 1993: The seasonal cycle of low stratiform clouds. *J. Climate*, **6**,  
474 1587–1606.
- 475 Kubar, T. L., and D. L. Hartmann, 2009: Understanding the importance of microphysics and  
476 macrophysics for warm rain in marine low clouds. Part I: Satellite observations. *J. Atmos.*  
477 *Sci.*, **66**, 2953–2972, doi:10.1175/2009JAS3071.1.
- 478 L’Ecuyer, T. S., and G. L. Stephens, 2002: An estimation-based precipitation retrieval algorithm  
479 for attenuating radars, *Journal of Applied Meteorology*, **41**(3), 272–285.
- 480 Larson, V. E., and D. P. Schanen, 2013: The Subgrid Importance Latin Hypercube Sampler  
481 (SILHS): a multivariate subcolumn generator, *Geosci. Model Dev.*, **6**(5), 1813–1829,  
482 doi:10.5194/gmd-6-1813-2013.
- 483 Lebsock, M., and H. Su, 2014: Application of active spaceborne remote sensing for  
484 understanding biases between passive cloud water path retrievals. *J. Geophys. Res. Atmos.*,





- 485        **119**, 8962–8979, doi:10.1002/2014JD021568.
- 486    Lebsock, M., H. Morrison, and A. Gettelman, 2013: Microphysical implications of cloud-  
487        precipitation covariance derived from satellite remote sensing, *J. Geophys. Res. Atmos.*, **118**,  
488        6521–6533, doi:10.1002/jgrd.50347.
- 489    Ma, P.-L., and Coauthors, 2013: The role of circulation features on black carbon transport into  
490        the Arctic in the Community Atmosphere Model version 5 (CAM5). *J. Geophys. Res. Atmos.*  
491        **118**, 4657–4669, doi:doi:10.1002/jgrd.50411.
- 492    Ma, P.-L., and Coauthors, 2015: How does increasing horizontal resolution in a global climate  
493        model improve the simulation of aerosol-cloud interactions? *Geophys. Res. Lett.*,  
494        **42**(12):5058–5065. doi:10.1002/2015GL064183.
- 495    Marchand, R., G. G. Mace, T. Ackerman, and G. Stephens, 2008: Hydrometeor detection using  
496        Cloudsat — An earth-orbiting 94-GHz cloud radar. *Journal of Atmospheric and Oceanic*  
497        *Technology*, **25**, 519–533, doi:10.1175/2007JTECHA1006.1.
- 498    Marchand, R., J. Haynes, G. G. Mace, T. Ackerman, and G. Stephens, 2009: A comparison of  
499        simulated cloud radar output from the multiscale modeling framework global climate model  
500        with CloudSat cloud radar observations. *J. Geophys. Res. Atmos.*, **114**,  
501        doi:10.1029/2008JD009790.
- 502    Morrison, H., and A. Gettelman, 2008: A new two-moment bulk stratiform cloud microphysics  
503        scheme in the community atmosphere model, version 3 (CAM3). Part I: Description and  
504        numerical tests. *J. Climate*, **21**, 3642–3659.
- 505    Nam, C., S. Bony, J. L. Dufresne, and H. Chepfer, 2012: The “too few, too bright” tropical low-  
506        cloud problem in CMIP5 models. *Geophys. Res. Lett.*, **39**, L21801,  
507        doi:10.1029/2012GL053421.
- 508    Neale, R. B., and Coauthors, 2010: Description of the NCAR community atmosphere model  
509        (CAM 5.0), *Tech. Rep. TN-486+STR*, 268 pp., *Natl. Cent. for Atmos. Res.*, Boulder, Colo.
- 510    Pincus, R., S. Platnick, S. A. Ackerman, R. S. Hemler, and R. J. Patrick Hofmann, 2012:  
511        Reconciling simulated and observed views of clouds: MODIS, ISCCP, and the limits of  
512        instrument simulators. *J. Climate*, **25**, 120220120058001, doi:10.1175/JCLI-D-11-00267.1.
- 513    Platnick, S., and Coauthors, 2017: The MODIS cloud optical and microphysical products:  
514        Collection 6 updates and examples from Terra and Aqua, *IEEE Transactions on Geoscience*  
515        *and Remote Sensing*, **55**(1), 502–525, doi:10.1109/TGRS.2016.2610522.
- 516    Randall, D., M. Khairoutdinov, A. Arakawa, and W. Grabowski, 2003: Breaking the cloud  
517        parameterization deadlock, *Bull. Am. Meteorol. Soc.*, **84**(11), 1547–1564.
- 518    Randall, D., M. Branson, M. Wang, S. Ghan, C. Craig, A. Gettelman, and J. Edwards, 2013: A



- community atmosphere model with superparameterized clouds, *Eos Trans. AGU*, **94**(25), 221–222.
- Song, H., Z. Zhang, P.-L. Ma, S. Ghan, M. Wang, 2017: An Evaluation of Marine Boundary Layer Cloud Property Simulations in Community Atmosphere Model Using Satellite Observations: Conventional Sub-grid Parameterization vs. CLUBB. *J. Climate*, In Press.
- Stephens, G. L., and Coauthors, 2002: The CloudSat Mission and the A-Train, *Bull. Am. Meteorol. Soc.*, **83**(12), 1771–1790, doi:10.1175/BAMS-83-12-1771.
- Stevens, B., G. Vali, K. Comstock, R. Woods, M. C. Van Zanten, P. H. Austin, C. S. Bretherton, and D. H. Lenschow, 2005: Pockets of open cells and drizzle in marine stratocumulus. *Bull. Am. Meteorol. Soc.*, **86**, 51–57.
- Suzuki, K., G. Stephens, A. Bodas-Salcedo, M. Wang, J.-C. Golaz, T. Yokohata, and T. Koshiro, 2015: Evaluation of the warm rain formation process in global models with satellite observations, *J. Atmos. Sci.*, **72**, 3996–4014, doi:10.1175/JAS-D-14-0265.1.
- Swales, D. J., R. Pincus, and A. Bodas-Salcedo, 2018: The Cloud Feedback Model Intercomparison Project Observational Simulator Package: Version 2, *Geosci. Model Dev.*, **11**, 77–81, <https://doi.org/10.5194/gmd-11-77-2018>.
- Takahashi, H., M. Lebsock, K. Suzuki, G. Stephens, and M. Wang, 2017: An investigation of microphysics and subgrid-scale variability in warm-rain clouds using the A-Train observations and a multiscale modeling framework. *J. Geophys. Res. Atmos.*, **122**(14), 7493–7504.
- Tanelli, S., S. L. Durden, E. Im, K. S. Pak, D. G. Reinke, P. Partain, J. M. Haynes, and R. T. Marchand, 2008: CloudSat's Cloud Profiling Radar After Two Years in Orbit: Performance, Calibration, and Processing, *IEEE TRANSACTIONS ON GEOSCIENCE AND REMOTE SENSING*, **46**(11), 3560–3573.
- Tao, W. K., and Coauthors, 2009: A multiscale modeling system developments, applications, and critical issues, *Bull. Am. Meteorol. Soc.*, **90**(4), 515–534.
- Wang, M., V. Larson, S. Ghan, M. Ovchinnikov, D. Schanen, H. Xiao, X. Liu, Z. Guo, and P. Rasch, 2015: A multiscale modeling framework model (superparameterized CAM5) with a higher-order turbulence closure: Model description and low-cloud simulations, *Journal of Advances in Modeling Earth Systems*, **7**, 484–509, doi:10.1002/2014MS000375.
- Wang, M., and Coauthors, 2011: The multi-scale aerosol-climate model PNNL-MMF: Model description and evaluation, *Geosci. Model. Dev.*, **4**(1), 137–168.
- Webb, M., C. Senior, S. Bony, and J. Morcrette, 2001: Combining ERBE and ISCCP data to assess clouds in the Hadley Centre, ECMWF and LMD atmospheric climate models. *Climate Dyn.*, **17**, 905–922.



554 Wood, R., 2005: Drizzle in stratiform boundary layer clouds. Part I: Vertical and horizontal  
555 structure. *J. Atmos. Sci.*, **62**, 3011–3033.

556 Zhang K., and Coauthors, 2014: Technical Note: On the use of nudging for aerosol-climate  
557 model intercomparison studies. *Atmospheric Chemistry and Physics*, **14**(16): 8631-  
558 8645. doi:10.5194/acp-14-8631-2014.

559 Zhang, Y., S. A. Klein, J. Boyle, and G. G. Mace, 2010: Evaluation of tropical cloud and  
560 precipitation statistics of Community Atmosphere Model version 3 using CloudSat and  
561 CALIPSO data. *J. Geophys. Res. Atmos.*, **115**, D12205, doi:10.1029/2009JD012006.

562

563

564

565

566

567

568

569

570

571

572

573

574

575

576

577

578

579

580



581 **List of Figures:**

582 Figure 1. a) PDF of rainwater mixing ratio for rainwater when the horizontal variability of  
583 rainwater is assumed to follow the exponential distribution. The vertical dashed blue line  
584 indicates the mean value of rainwater mixing ratio as 0.03 g/kg. b) The corresponding PDF  
585 of the CloudSat radar reflectivity simulated by COSP assuming the Marshall and Palmer  
586 particle size distribution. The dashed blue line corresponds to the radar reflectivity based on  
587 the mean rainwater 0.03 g/kg, and the solid red line corresponds to the grid-mean radar  
588 reflectivity based on the PDF of rainwater mixing ratio.

589 Figure 2. a) The grid mean total (stratiform plus convective) and convective cloud fraction. b) the  
590 grid mean mixing ratios of cloud and precipitation hydrometeors (LS\_CLIQ: large-scale (i.e.,  
591 stratiform) cloud water; LS\_CICE: large-scale cloud ice; LS\_RAIN: large-scale rain;  
592 LS\_SNOW: large-scale snow; LS\_GRPL: large-scale graupel; CV\_CLIQ: convective cloud  
593 water; CV\_CICE: convective cloud ice; CV\_RAIN: convective rain; CV\_SNOW: convective  
594 snow). c) the distribution of large-scale and convective cloud among the sub-columns  
595 generated by the SCOPS scheme (i.e., frac\_out from scops.f). d) the distribution of large-  
596 scale and convective precipitation among the sub-columns generated by the SCOPS-PREC  
597 scheme (i.e., prec\_frac from prec\_scops.f). e) the mixing ratio (left panels) and effective  
598 radius (right panels) of three hydrometeor types among the sub-columns.

599 Figure 3. Tropical averaged radar reflectivity-height histogram in the CloudSat observation (top),  
600 the SPCAM5 CloudSat simulation (bottom left) and the SPCAM5\_Homogeneous CloudSat  
601 simulation (bottom right).



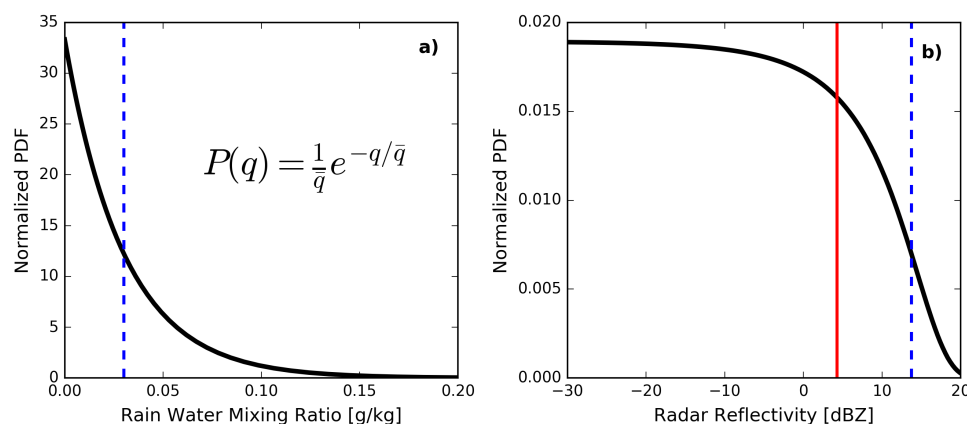
Figure 4. The histograms of column maximum radar reflectivity for liquid clouds over oceanic regions from 45°S to 45°N in A-Train satellite observations, SPCAM5 COSP and SPCAM5-Homogeneous COSP simulations.

Figure 5. Probability of precipitation (POP) of liquid clouds between 500hPa and 900hPa levels in the satellite observations (left panel), the SPCAM5 COSP simulation (middle panel) and the SPCAM5-Homogeneous COSP simulation (right panel). Three categories of precipitation: drizzle plus rain (column  $Z_{\max} > -15$  dBZ, top panels), rain (column  $Z_{\max} > 0$  dBZ, middle panels), and strong rain only (column  $Z_{\max} > 10$  dBZ, bottom panels). Unit of POP is %.

Figure 6. POP (drizzle or rain) of liquid clouds at each LWP and liquid cloud effective radius in the satellite observations (top), the SPCAM5 COSP simulation (bottom left) and the SPCAM5-Homogeneous COSP simulation (bottom right). The white solid contours are joint PDF of LWP and liquid cloud effective radius. Units of POP and PDF are %.



625



626

627

628 Figure 1. a) PDF of rainwater mixing ratio for rainwater when the horizontal variability of rainwater is assumed to  
 629 follow the exponential distribution. The vertical dashed blue line indicates the mean value of rainwater mixing ratio  
 630 as 0.03 g/kg. b) The corresponding PDF of the CloudSat radar reflectivity simulated by COSP assuming the  
 631 Marshall and Palmer particle size distribution. The dashed blue line corresponds to the radar reflectivity based on  
 632 the mean rainwater 0.03 g/kg, and the solid red line corresponds to the grid-mean radar reflectivity based on the PDF  
 633 of rainwater mixing ratio.

634

635

636

637

638

639

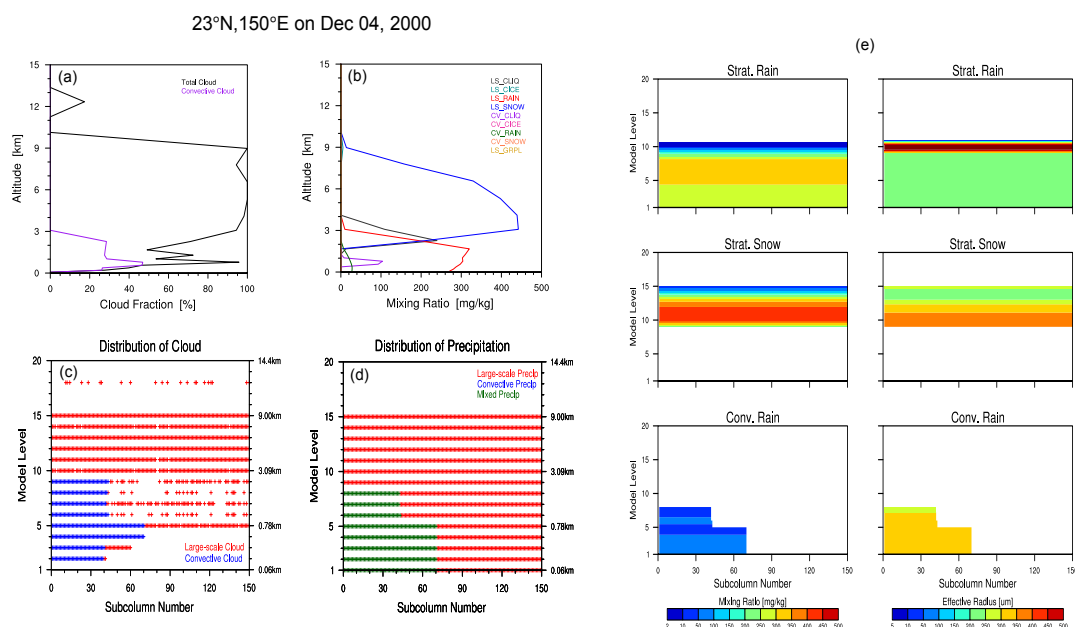
640

641

642



643



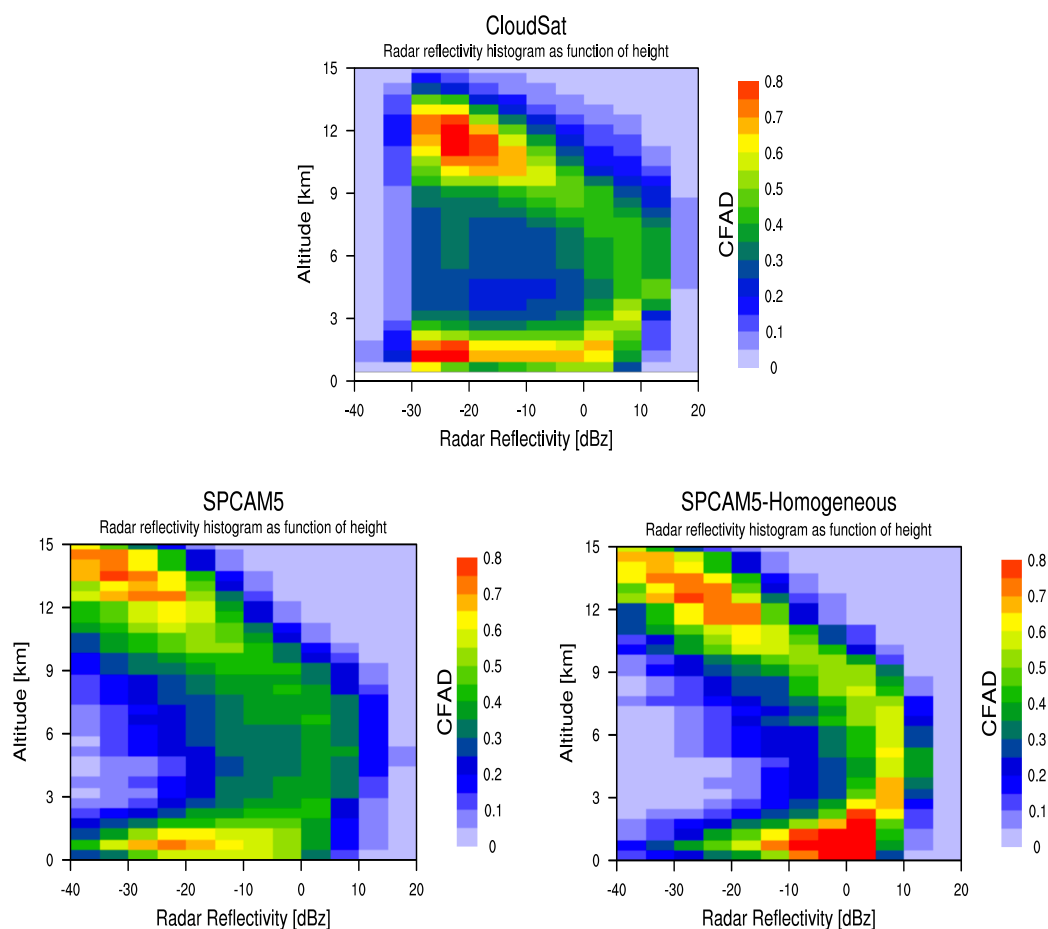
644

645

646 Figure 2. a) The grid mean total (stratiform plus convective) and convective cloud fraction. b) the  
 647 grid mean mixing ratios of cloud and precipitation hydrometeors (LS\_CLIQ: large-scale (i.e.,  
 648 stratiform) cloud water; LS\_CICE: large-scale cloud ice; LS\_RAIN: large-scale rain;  
 649 LS\_SNOW: large-scale snow; LS\_GRPL: large-scale graupel; CV\_CLIQ: convective cloud  
 650 water; CV\_CICE: convective cloud ice; CV\_RAIN: convective rain; CV\_SNOW: convective  
 651 snow). c) the distribution of large-scale and convective cloud among the sub-columns generated  
 652 by the SCOPS scheme (i.e., frac\_out from scops.f). d) the distribution of large-scale and  
 653 convective precipitation among the sub-columns generated by the SCOPS-PREC scheme (i.e.,  
 654 prec\_frac from prec\_scops.f). e) the mixing ratio (left panels) and effective radius (right panels)  
 655 of three precipitation hydrometeor types among the sub-columns.



656



657

658

659 Figure 3. Tropical averaged radar reflectivity-height histogram in the CloudSat observation (top),  
 660 the SPCAM5 COSP simulation (bottom left) and the SPCAM5-Homogeneous COSP simulation  
 661 (bottom right).

662

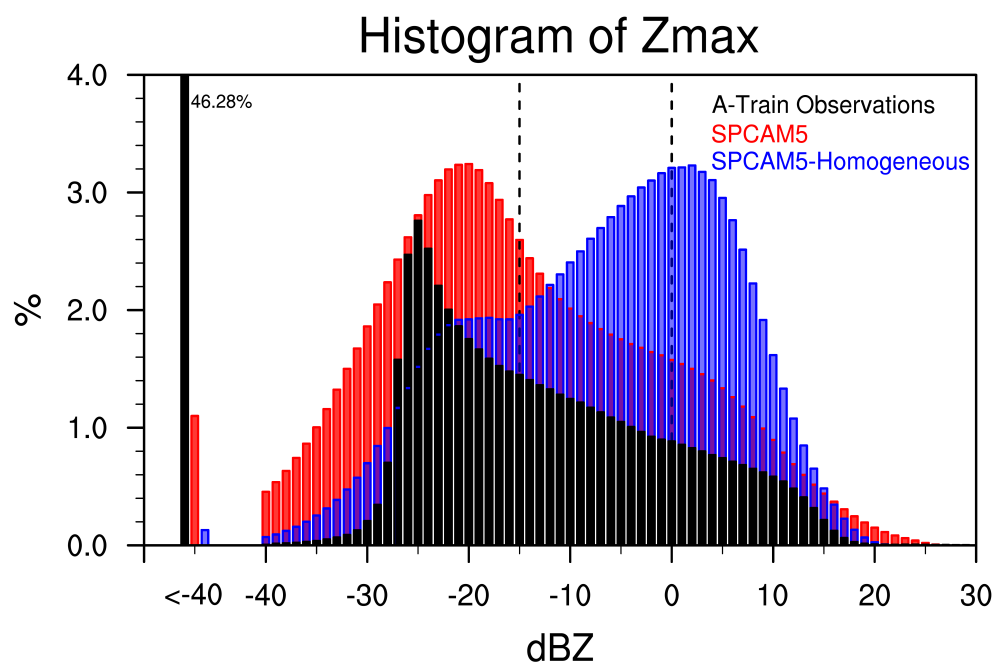
663

664





665



666

667

668 Figure 4. The histograms of column maximum radar reflectivity for liquid clouds over oceanic  
 669 regions from 45°S to 45°N in A-Train satellite observations, SPCAM5 COSP and SPCAM5-  
 670 Homogeneous COSP simulations.

671

672

673

674

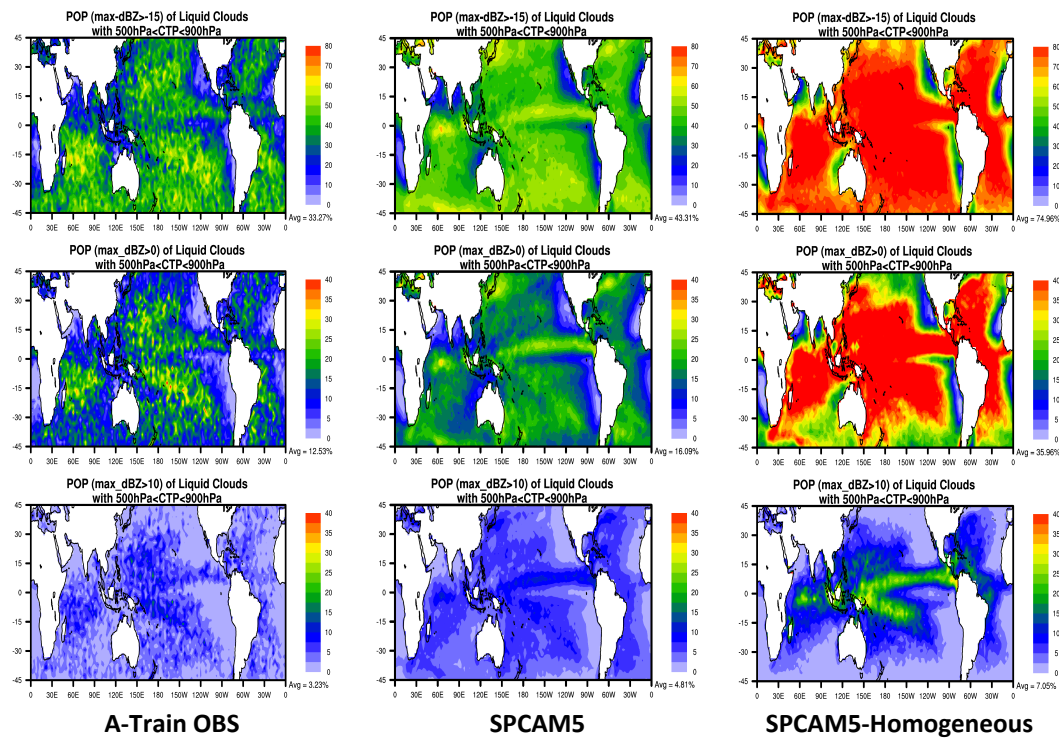
675

676

677



678



679

680

681 Figure 5. Probability of precipitation (POP) of liquid clouds between 500hPa and 900hPa levels  
682 in the satellite observations (left panel), the SPCAM5 COSP simulation (middle panel) and the  
683 SPCAM5-Homogeneous COSP simulation (right panel). Three categories of precipitation:  
684 drizzle plus rain (column  $Z_{\max} > -15$  dBZ, top panels), rain (column  $Z_{\max} > 0$  dBZ, middle  
685 panels), and strong rain only (column  $Z_{\max} > 10$  dBZ, bottom panels). Unit of POP is %.

686

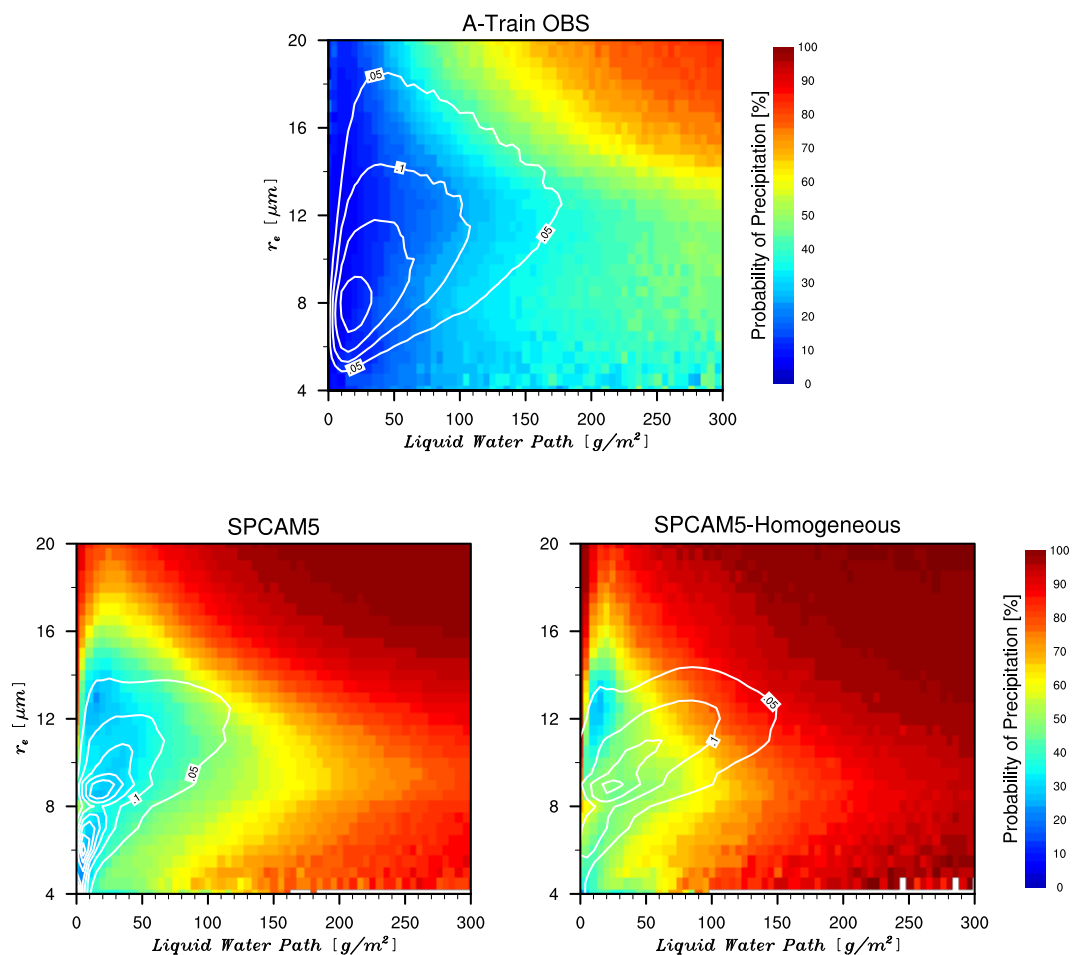
687

688

689



690



691

692

693 Figure 6. POP (drizzle or rain) of liquid clouds at each LWP and liquid cloud effective radius in  
 694 the satellite observations (top), the SPCAM5 COSP simulation (bottom left) and the SPCAM5-  
 695 Homogeneous COSP simulation (bottom right). The white solid contours are joint PDF of LWP  
 696 and liquid cloud effective radius. Units of POP and PDF are %.